POLİTEKNİK DERGİSİ

JOURNAL of POLYTECHNIC

ISSN: 1302-0900 (PRINT), ISSN: 2147-9429 (ONLINE)
URL: http://dergipark.gov.tr/politeknik

On the compression properties and erosion-corrosion behavior of Al 6061/15%Sic$_p$ composite

***Yazar(lar) (Author(s))**: Osama M. IRFAN[1] , Abdulaziz S. ALABOODİ[2]*

ORCID[1]: 0000-0002-9104-1611

ORCID[2]: 0000-0003-0370-5324

Bu makaleye şu şekilde atıfta bulunabilirsiniz (To cite to this article): Irfan, O. M. And Alaboodi A. S., "On the compression properties and erosion-corrosion behavior of Al 6061/15%Sicp composite", ***Politeknik Dergisi***, 23(2): 415-425, (2020).

Erişim linki (To link to this article): http://dergipark.gov.tr/politeknik/archive

DOI: **10.2339/politeknik.535022**

On the Compression Properties and Erosion-Corrosion Behaviour of Al 6061/15%Sic$_p$ Composite

Araştırma Makalesi / Research Article

Osama M. IRFAN[1, 2*], Abdulaziz S. ALABOODİ[1]

[1]Department of Mechanical Engineering, Qassim University, Buraidah, Saudi Arabia

[2]Beni Suef University, Beni Suef, Egypt

(Received : 04.03.2019 ; Accepted : 22.05.2019)

ABSTRACT

Aluminum alloys and composites are used in automobile and aerospace industries due to good mechanical properties, higher corrosion resistance and light weight. The compression test of materials at elevated temperature is useful to study the flow stress, workability, and the analysis of the processing conditions. In this paper, ring specimens produced from Al 6061/15%SiC$_p$ composite were subjected to uniaxial hot compression tests to invistigate the deformation behavior of the material. The tests were performed at high temperatures ranged from 300 ^{o}C to 500 ^{o}C and strain rates of 0.008 s^{-1} to 2.7 s^{-1}. The flow stress-strain curve at different strain rates and temperatures was determined. The regression analysis was performed to predict the flow stress during the compression test. The comparison between the experimental and theoretical results was also conducted. In addition, finite element method was applied to simulate and validate the compression behavior of the composite ring. Furthermore, the erosion-corrosion tests by slurry pot method were conducted to examine the influence of SiC particles on erosion corrosion resistance of the material. The results showed that the flow stress of the Al6061/15/vol.%SiC$_p$ composite is correlated directly with temperature and strain rate. Also, the erosion corrosion resistance increased with adding SiC particles to Al 6061 alloy.

Keywords: Al6061% SiC composite, compression test, flow stress, finite element modeling; erosion-corrosion.

1 INTRODUCTION

Aluminum-based composites have extensive applications in various industries including aerospace, automotive, and electronics due to their superior properties such as high stiffness, low density, and good wear resistance [1 and 2].Various methods are used to produce a reinforced aluminum-based composite, such as casting processes, spray deposition and powder metallurgy techniques [3-6]. The reinforcement by alumina (Al_2O_3) and silicon carbide (SiC) affects the mechanical properties and workability of the composites [7-9]. However, the deformation of composite materials at room temperature is challenging due to reduced plasticity, high hardening rate, and less elongation; thus, investigation of the hot deformation behavior is very important [10]. The importance of bulk metal working is due to two primary reasons. First, the changes of major microstructural occur influencing the subsequent processing. Secondly, the improvement of processing techniques has highly effective on the overall manufacturing productivity[11]. Recently the hot compression test was employed in many researches. In particular, for large strains with lubrication; uniform deformation can be achieved. Moreover, the compressive state represents the conditions present in forging, extrusion and rolling process [12]. The flow stress-strain curve of plastic metals are dominated by the comparison between recovery mechanisms and strain hardening. When large deformations strains at elevated temperatures had occurred, the dynamic recrystallization and texture formation may influence the flow behavior[13]. A smaller grain size is generally associated with greater strength, hardness, and ductility. The recrystallization is the mechanism, which results in fine grain structure in hot working. Dynamic recrystallization occurs only during hot working of metals. The process parameters that affect the recrystallization process are the temperature, strain, and strain rate [14]. Until now trial and error, techniques have been in practice for optimizing and designing the bulk metal working processes. Now they are being replaced by modeling techniques for accuracy [15]. Considerable research works have been conducted on computer modeling to characterize the deformation of material at high temperature. Yet, most of the plastic behavior relations are empirical and not based on a particular theoretical approach. However, the Holloman equation is broadly used to approximate the steel plastic behavior. It is adequately accurate to describe the stress-strain curve at low strains [16]. Recent researchers have employed an equation that relating critical strain to initial grain size and Zener-Holloman parameter to calculate the dynamic recrystallization onset. There are significant alterations in the applied expressions to determine the grain size after recrystallization and in their behavior of specific materials [16]. Some researchers have employed the proposed equations for recrystallized grain size for their model [17]. Considerable efforts were exerted previously focusing on the fabrication and deformation of aluminum-based composites but a few have studied the compression behavior of aluminum composites. For example, SiC$_p$ reinforced Al 2080 matrix composite was fabricated by Srivatsan and Prakash by using dry blending techniques [18 and 19]. Hung et al. produced Al/SiC$_p$/359 composite by permanent mold casting

*Sorumlu yazar (Corresponding Author)
e-mail: osamaerfan@qec.edu.sa

technique [20]. SiC_p reinforced Al 2014 and Al 6061 composites were fabricated by Song et al. [21]. The process of vertical pressure casting [22] fabricated SiC-reinforced Al 7075 composite. Rao et al applied solidification processing by stir casting to produce Al-Zn-Mg-SiC_p composite [23]. The mechanical wear of aluminum based alloy was investigated by many researchers [24 and 25]. Suresh et al. [26] studied the wear of stir cast Al-TiB2 composites. Umanath et al. [27] examined the mechanical wear of Al6061/SiC/Al_2O_3 composites with deferent reinforcement percentages. The results showed better wear resistance of 15% composites compared to 5% composites. Yet, the erosion corrosion resistance of Al 6061 alloy and Al 6061/SiC composites was not investigated.

The aim of the current paper is to produce Al 6061/15%/SiC_p composite by dry blending technique. The microstructure of both Al 6061 alloy and Al 6061/15%/SiC_p composite were investigated. Then the work focused on measuring and predicting the flow stress of ring specimens during hot deformation. A comparison between the measured and predicted results was carried out. A finite element method was applied for modeling the compression behavior of the produced composite. Moreover, the erosion corrosion behaviours of both Al 6161 alloy and Al 6061/ 15% SiC_p composite were studied to evaluate the surface proprties of both materials.

2. MATERIAL and METHOD

The materials used in this work are aluminium alloy powder and silicon carbide (SiC_p) particulates that were purchased from Baoding Yuankun Machinery Manufacturing Co. Ltd, China. The aluminium powder and particulates SiC_p (15 vol. %) were mixed with 1% zinc stearate in a vacuum powder-mixing chamber. The blending of the components was done by a double cone stirrer. Then the mixture was compacted with a pressure of 170 MPa in a forming die made from steel H13. The compacts were heated to 150 ºC for 2 hours and degassing was implemented by placing the compact in a vacuum chamber and heating it to 270 ºC for 4 hours. The sintering process was carried out at 540 ºC for 4 hours. The chemical composition of Al 6061 alloy utilized in the current study is given in Table 1. Compression ring specimens were prepared through a CNC machine under cooling condition. Using a ring specimen was to reduce the required compression stress.

Table 1. Chemical composition of AL 6061 alloy

Element	Mn	Cr	Fe	Cu	Si	Mg	Ti	Zn	Al
Wt.%	0.1	0.05	0.6	0.2	0.5	0.9	0.1	0.1	Bal

2.1 Compression Test

Sets of compression tests according to ASTM E9 at elevated temperature were performed for Al 6061/15%SiC_p composite ring specimens. A universal testing machine with a capacity of 10 Tonnes having FIE-Unitek servo controller was used for the experiments. The shape and dimensions of the test specimens are illustrated in Fig. 1 and the setup of the compression test is shown in Fig. 2. The upper and lower surfaces of the specimens were lubricated by temperature resistance graphite lubricant to reduce the friction effect during the compression test. The deformation was carried out to a true strain ranging from 0.1 to 0.5. Then the specimens were heated in an electrical resistance split type muffle furnace. A thermocouple of 1.0 mm diameter was used to monitor the temperature. For more accuracy, a laser gun device was also used to measure the temperature. The compression tests were conducted at a temperature ranges from 300 ºC to 500 ºC with a step of 50 ºC and strain rate (έ) ranges from 0.008 s^{-1} to 2.7 s^{-1}.

The specimens were compressed to a true strain of 0.5 then quenched in cold water. The volume constancy principle was applied to calculate the true stress and true strain of the ring specimen.

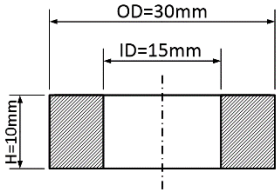

Fig. 1. Al 6061/15%SiC_p composite ring specimen

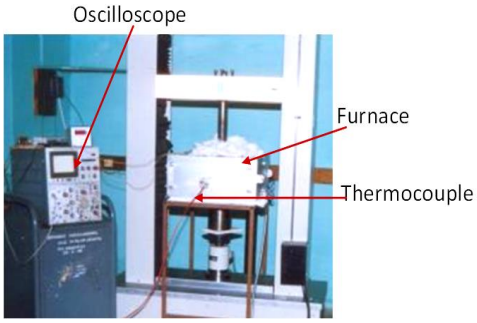

Fig. 2. Set up of the compression test

The actual area of the ring that subjected to compression stress can be obtained by the following formula:

$$A_o = \frac{\pi}{4}\left(OD^2 - ID^2\right) \quad (1)$$

Where OD and ID are outer diameter and inner diameter of ring respectively.

$$\textit{Volume of the specimen} = \textit{Area x Height} \quad (2)$$

$$\textit{Instantaneous height } (h_i) = h_o - \delta.h \quad (3)$$

Where h_o is initial height and δ.h is the change in height due to deformation. By using volume constancy principle,

$$A_i\, h_i = A_o\, h_o, \textit{ and hence} \quad A_i = A_o\, h_o/h_i \quad (4)$$

The flow stress is the resistance against deformation to the applied load. It is the instantaneous response of the material to the applied load as represented in Eq. (5) [28].

$$\sigma_T = P_i/A_i \quad (5)$$

Where σ_T is True stress, P_i is instantaneous load, and Ai is instantaneous area. True strain is the logarithmic relation of change in height to the original height. The true strain is obtained by Eq. (6) [29].

$$True\ strain\ (\varepsilon) = ln\ h_o/h_i \quad (6)$$

2.2 Erosion-corrosion Experiments

The slury pot method was used for conducting the erosion corrosion tests of Al 6061 alloy and Al 6061/15%SiC_p samples in a saline water following the ASTM G119 standard. The details of test rig and samples prepartion were described earlier elsewhere [30]. Samples of Al 6061 alloy and Al 6061/15%SiC_p composities were tested in two different media; namely 3.5 wt.% NaCl solution (for corrosion) and 3.5 wt.% NaCl slurry containing 20 wt.% of erosive particles (for erosion-corrosion). Silica sand with average size of $250^{\pm 40}$ µm was used as erosive elements. A digital balance with a resolution of 0.1 mg was utilized to weigh the samples before and after the erosion corrosion experiments. The weight loss per unit area was computed and considered as an indication of erosion corrosion effect. The erosion corrosion behaviors of Al 6061 alloy and Al 6061/15%SiC_p were investigated at various durations and flow velocities. Three samples were tested for each condition and the average weight loss per unit area was reported. The surface degradation was examined by optical microcope and scanning electron microscope (SEM).

3. RESULTS AND DISCUSSION

3.1. Microstructure Investigation

The microstructure of Al 6061 alloy and 6061 Al/15%/SiC_p composites samples were investigated with optical microscope (Fig.3) and scanning electron microscope (SEM) (Fig.4). Before investigation, the samples were ground, polished and etched as followed: The grinding was carried out by using emery paper with the different grits of (400, 600, 800 and 1000). Polishing was implemented by using diamond paste (1µm size). Etching was done by a solution (95% H_2O + 1%HF). Then the samples were cleaned with water and alcohol. The images indicate that the reinforcement material (SiC_p) is distributed uniformlyand and good bonding between the Al 6061 matrix alloy and SiC particles is exiting. Fig.5 presents the X-ray diffraction (XRD) analysis that showing the presence of SiC particles in the alloy matrix as small peaks. These results are in agreement with findings of previous researchers [8, 9, and 31 – 34]. After compression, the microstructures of both alloy and composite were investigated again to identify the alterations due to deformation. It was observed that at high temperature and low speed, the materials with stable structures exhibited abnormal elongation. Superplastic deformation was noticed and grain boundary sliding occurred at a rate in which the cracks can be repaired. This behaviour is similar to other materials like brass and Mg-Li alloys [32]. It is well known that, at elevated temperatures and low strain rates, the grain boundary sliding occurs under shear stress.

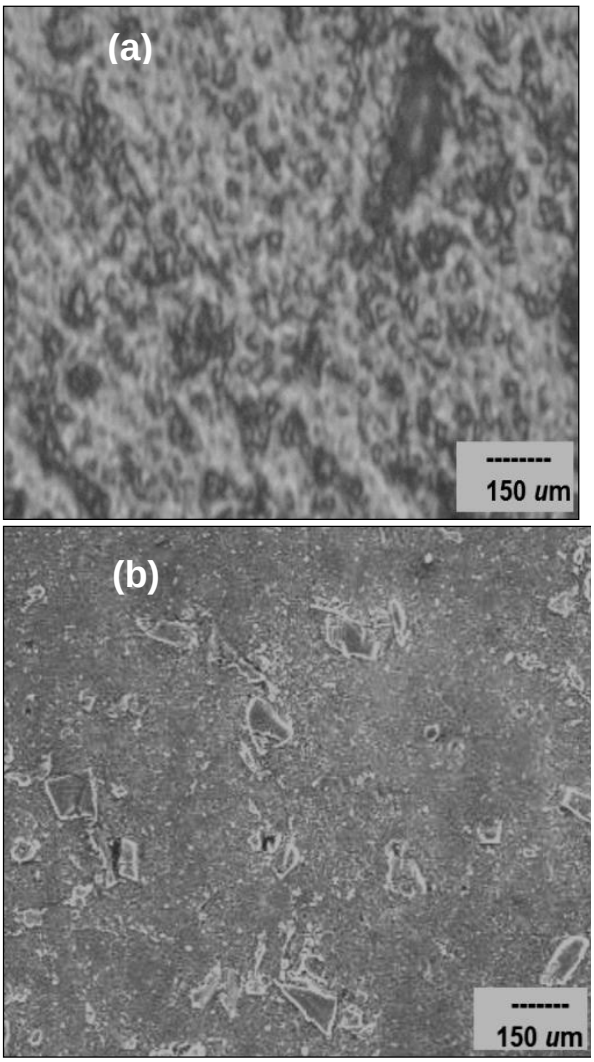

Fig. 3. Microstructure by optical microscopy
(a) Al 6061 alloy, (b) Al 6061 /15%/SiC_p Composites

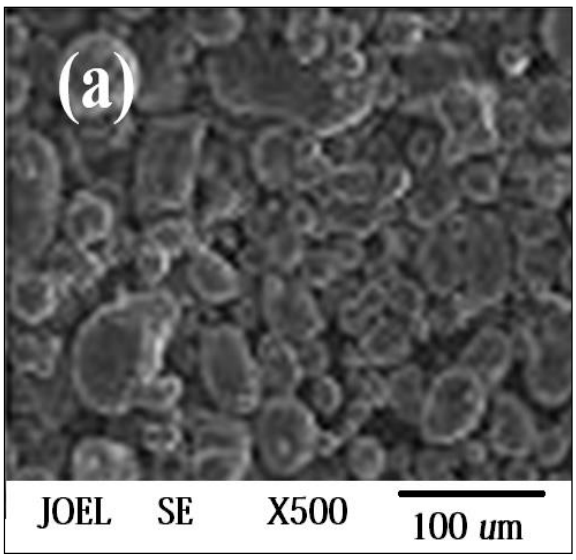

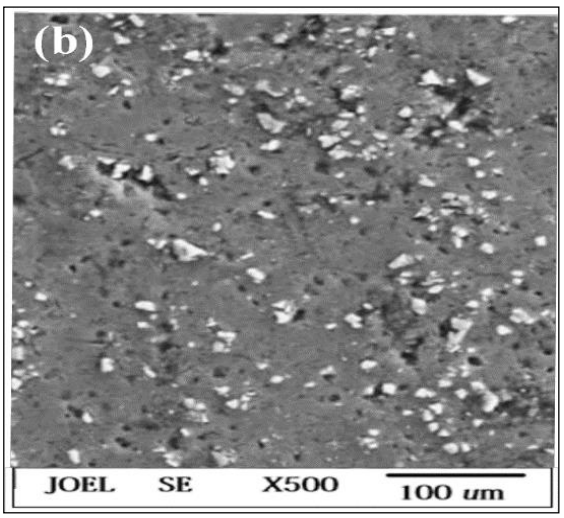

Fig. 4. Microstructure by SEM (a) Al 6061 alloy, (b) Al 6061 /15%/SiCp Composites

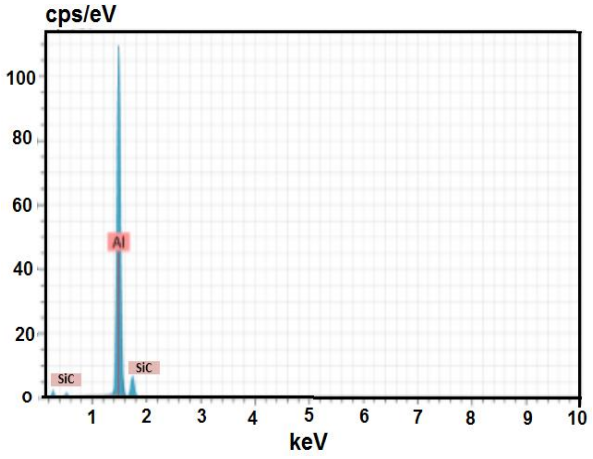

Fig.5. X-Ray diffraction (XRD) of Al 6061 /15%/SiCp Composites

Since the rate of diffusion is not rapid enough during the compression test, wedge cracks may appear at the grain boundary. The wedge cracks can be controlled or decreased by raising the strain rate or reducing the temperature. Superplastic deformation may also lead to interface cracking as shown in Fig.6.

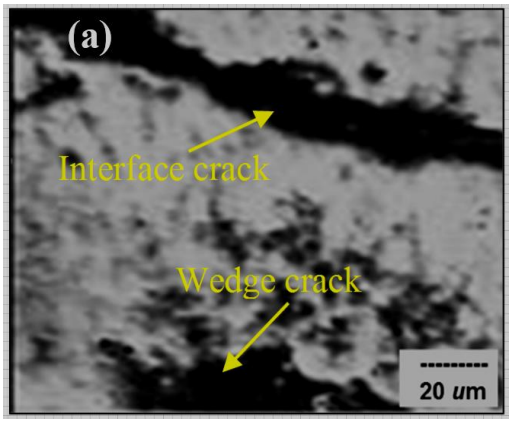

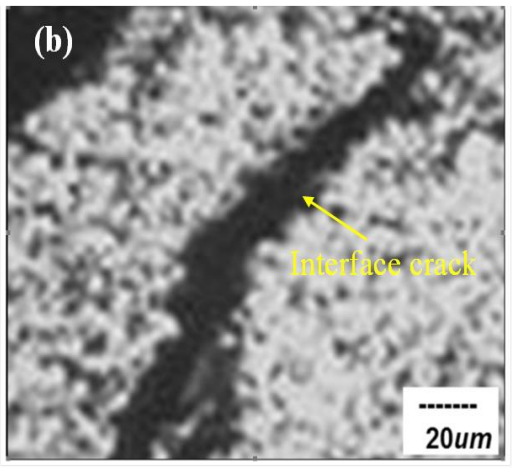

Fig. 6. Optical images of interface cracking; (a) at 300 ºC and strain rate of 0.008 s^{-1} (b) at 450 ºC and strain rate 0.4 s^{-1}

3.2. Flow Stress-Strain Investigation

The flow curves (from 300 ºC and 500 ºC) at different strain rates for Al 6061/15/ vol. % SiC_p are shown Fig. 7 through Fig. 11. It is clear that the strain rate has a dominant effect on the flow stress. All curves reach the maximum values and achieve the condition of steady state with increase of strain rates. With lower strain rates (0.05 s^{-1} and 0.008 s^{-1}) the maximum stress value was not achieved. The variation in the flow stress at low strain rates is not significant. This means that at higher strain rates a reduction of work hardening occurs. At relatively low temperatures of 300 ºC and 350 ºC, the strain hardening is high. Increasing the temperature results in decreasing the strain hardening. This explains the high strength and work hardening of the material at lower temperatures. The dislocation density resists the flow of the material and affects the strengthening mechanism. This leads to higher strain hardening. At higher temperatures (450 ºC and 500 ºC), the material became more ductile and has a softening behavior [33].

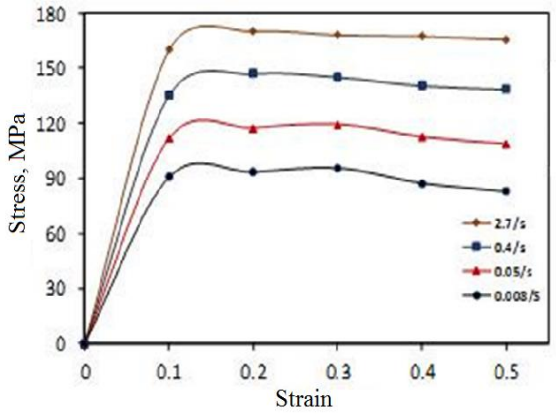

Fig. 7. Flow stress-strain of Al 6061/15/ vol. % SiC composite at 300 ºC

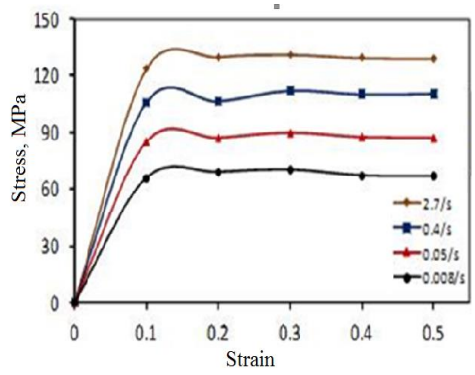

Fig. 8 Flow stress-strain of Al 6061/15/ vol. % SiC composite at 350 ºC

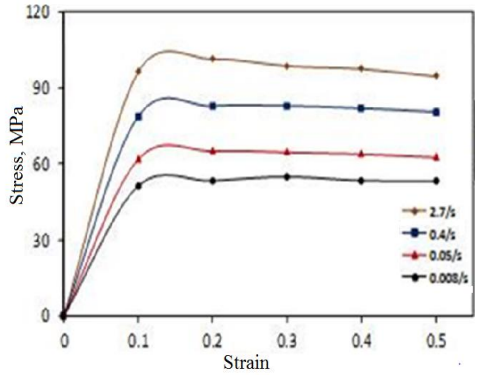

Fig. 9. Flow stress-strain of Al 6061/15/ vol. % SiC composite at 400 ºC

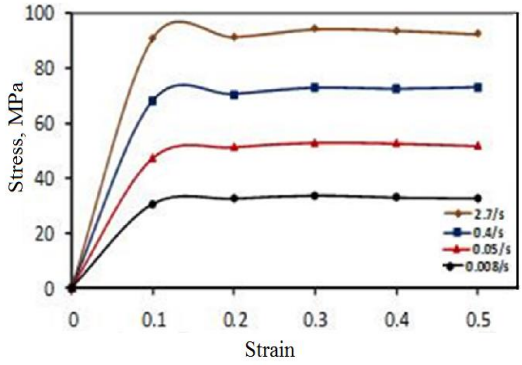

Fig. 10. Flow stress-strain of Al 6061/15/ vol. % SiC composite at 450 ºC

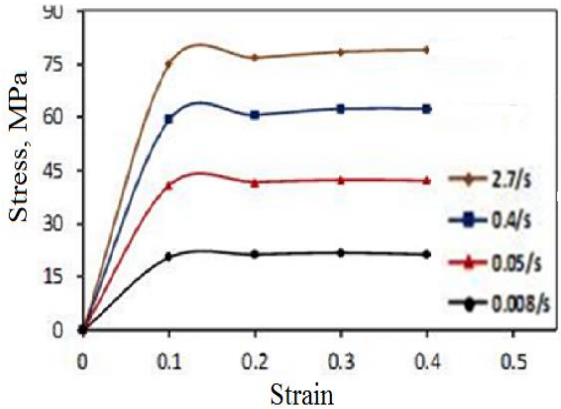

Fig.11. Flow stress-strain of Al 6061/15/ vol. % SiC composite at 500 ºC

It can be concluded that the flow stress is directly dependent on the strain rate. The stress raised rapidly during the initial stage and after accomplishment of maximum stress, a monotonic decrease occurs. Moreover, at higher strain rates (0.4 s^{-1} and 2.7 s^{-1}) the stress-strain curves reach the steady state with increasing the strain. For all cases, the increasing of temperature results in decreasing the flow stress of 6061Al/15%/SiC_p composite and extra energy was provided to the material due to higher temperatures. Therefore, dynamically recrystallized grains and dislocations were generated. Moreover, the increase of temperature decreases the adhesive strength between the SiC reinforcements and Al 6061 matrix. Thus, lower shear stress and dynamic recrystallization may reduce the flow stress at higher temperatures [35- 38].

3.3. Flow Stress Prediction

Regression method was used as an accurate statistical method for the analysis of data. In order to characterize the deformation behavior under different processing conditions in forming operation, an effective means of establishing the complicated relationship between the flow stress and the process variables may be sightseen. The regression analysis was applied to predict the flow stress of Al 6061/15%/SiC_p composite. The comparison between experimental and theoretical results was carried out. The prediction of flow stress was implemented through four steps: first; empirical model identification of the process, second: the model present parameters estimation as a function of strain, strain rate and temperature, third; flow stress prediction using empirical model, fourth; identification of mean deviation between the predicted and measured values of flow stress. Equation (7) shows the regression of the flow stress during hot deformation:

$$Z = \left(\dot{\varepsilon}\right) exp\left(\frac{Q}{RT}\right) = A[sinh(\sigma\alpha)]^n \qquad (7)$$

Where Z is Zener-Holloman parameter [16], ἑ is strain rate s^{-1}, Q is the activation energy for deformation (KJ/mole), R is gas constant (8.314 KJ/kg.mole.k), A and α are constants related to materials, and n is the stress exponent. Activation energy (Q) is the required energy for the atoms movement that described based on dynamic precipitation at the deformation stage. It can be calculated by using equation (8),

$$Q = \frac{kR}{m} \qquad (8)$$

Where k is the slope of (lnσ vs. 1/T) plots and m is the slope of (lnσ vs. lnε) plots. The values of k and m for different strains are shown in Table 3.

Table 3. Values of k and m at different strains

Strain	Slope	
	k	m
0.1	3.3	0.11
0.2	2.3	0.11
0.3	2.3	0.099
0.4	3.1	0.11
0.5	2.2	0.12

The model was modified to designate the flow stress of metals at high temperatures. Each parameter is considered as an independent variable that is a function of strain. For 6061 Al/15% SiC_p, the parameters Q, A, α, and n are obtained in terms of ε at different temperatures (300, 350, 400, and 450 °C) as follows:

$$Q = \begin{cases} 124.710 + 124.71\exp(-0.1(\varepsilon - 0.1)^2) \\ 86.971 + 86.884\exp\left(-0.0279(\varepsilon - 0.2788)^2\right) \\ 4.557 + 3.194\exp\left(3.542(\varepsilon + 0.7731)^2\right) \\ 117.678 + 116.619\exp\left(0.889(\varepsilon - 0.3957)^2\right) \\ 76.819 + 75.592\exp\left(1.099(\varepsilon - 0.5101)^2\right) \end{cases} \quad (9)$$

$$\ln A = \begin{cases} 5.015 + 2.799\exp\left(0.584(\varepsilon + 2.277)^2\right) \\ 4.092 + 2.693\exp\left(0.877(\varepsilon + 1.684)^2\right) \\ 4.228 + 2.994\exp\left(0.747(\varepsilon + 1.738)^2\right) \\ 4.473 + 3.407\exp\left(0.704(\varepsilon + 1.688)^2\right) \\ 4.400 + 3.491\exp\left(1.269(\varepsilon + 0.960)^2\right) \end{cases} \quad (10)$$

$$\alpha = \begin{cases} -0.022 + 0.757\exp\left(-1.300(\varepsilon + 1.542)^2\right) \\ -0.0003 + 0.0006\exp\left(-0.101(\varepsilon + 0.107)^2\right) \\ -0.018 + 0.836\exp\left(-1.279(\varepsilon + 1.43)^2\right) \\ -0.017 + 0.869\exp\left(-1.258(\varepsilon + 1.368)^2\right) \\ -0.002 + 0.002\exp\left(-0.104(\varepsilon + 0.101)^2\right) \end{cases} \quad (11)$$

$$n = \begin{cases} 5.120 + 4.053\exp\left(-0.388(\varepsilon - 0.331)^2\right) \\ 5.255 + 3.913\exp\left(-0.119(\varepsilon - 0.611)^2\right) \\ 5.815 + 4.135\exp\left(-0.047(\varepsilon + 0.805)^2\right) \\ 7.195 + 1.644\exp\left(0.384(\varepsilon - 1.009)^2\right) \\ 6.927 + 1.366\exp\left(0.377(\varepsilon - 0.768)^2\right) \end{cases} \quad (12)$$

The flow stress can be predicted by using equations 9 through 12 for different hot deformation conditions. Therefore, the predicted and measured flow stress was compared. It was obtained that the deviation of the predicted flow stress is more and the maximum deviation using regression method was almost 26.6 %. By observing the measured and predicted flow stress for the experimental data, mean deviation of 8.1% was obtained.

3.4. Modeling of Compression Behavior by Finite Element Method (FEM)

The finite element model was developed to study numerically and validate the stresses induced in the ring specimen during hot deformation. Quarter of the ring was modeled because of the similarity with the same dimension of ring conducted on experimental approach. The material properties were extracted from the experimental results. The friction coefficient between ring surface, upper pellet, and lower pellet was assumed to be minimum (μ = 0.05). The material properties was fed from the experimental results with similarity of the dimensions of the ring. Moreover, the material properties were obtained from the experimental results. The ring modeling is presented in Fig. 12 and Fig. 13. The variations of ring deformation in experiments as well as in simulation prove that the FEM model is valid. Furtheremore, the microstructure of the deformed ring (Fig. 3 and Fig. 4) indicated that no microscopic defects existed and the grains are distributed homogeneously. Therefore, the design of the ring is reasonable for experiements and simulation.

(a) (b) (c)

Fig. 12. (a) Ring between top and bottom pellet,
(b) the quarter of ring model,
(c) the mesh of quarter ring.

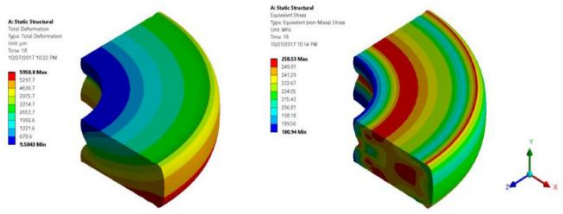

(a) (b)

Fig. 13. (a) ring deformation distribution on -y direction
(b) equivalent (von-Mises) stress distribution

3.5. Erosion Corrosion Results

3.5.1. Surface invistigation

The surfaces of Al 6061 alloy and Al 6061/15%SiC_p composite were investigated and compared by scaning electron microscope (SEM) to gain more understanding of the material removal mechanisms as a result of erosion corrosion. Positions near the center of the test samples were selected for observation. The micrographs of eroded corroded surfaces at deferent conditions are shown in Fig.14 and Fig.15. Fig.14a shows the surface of as received Al 6061 alloy before erosion corrosion experiments. Figs. 14b and 14c show the surfaces of Al 6061 alloy after corrosion and erosion-corrosion respectievely. It is clear that the surface degredation due to erosion corrosion is more sever than that generated by corrosion only. More grooves and bigger pits can be seen

as a result of erosion corrosion rather than corrosion only.

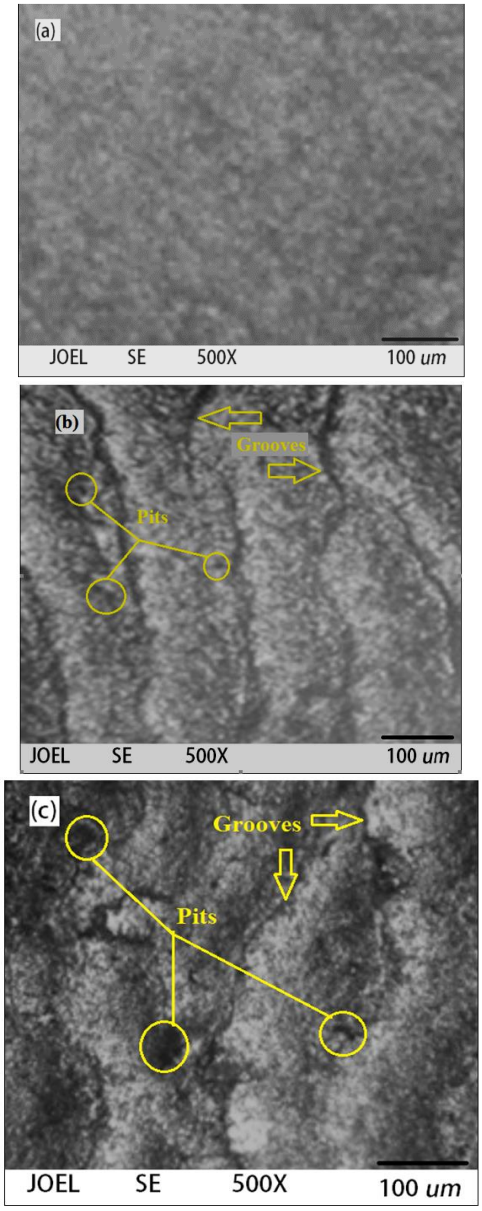

Fig. 14. Surface degradation of Al 6061 alloy
(a)before erosion-corsion ,
(b) after corrosion, and
(c) after erosion-corrosion

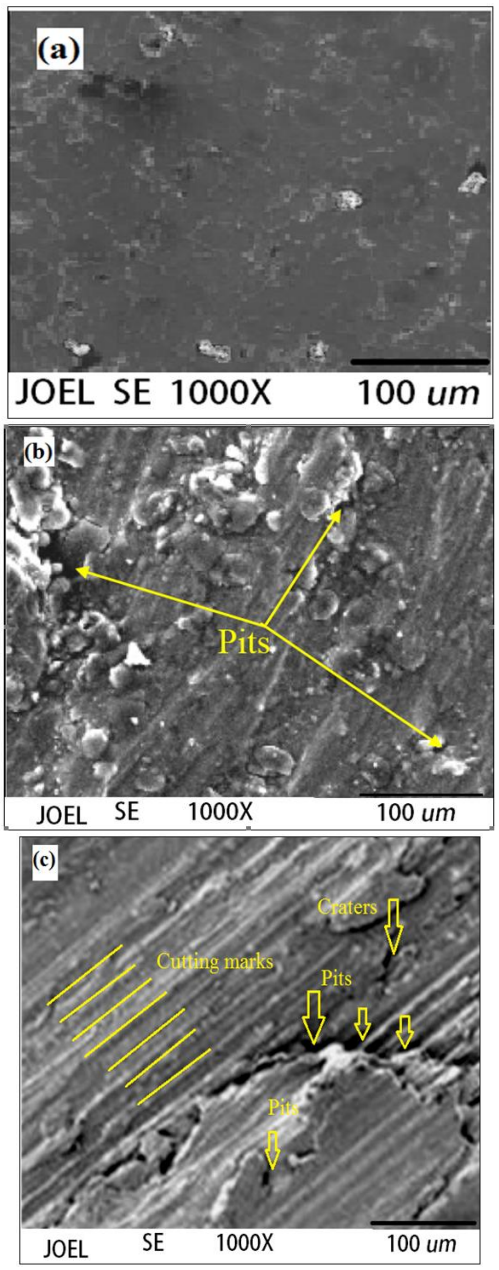

Fig. 15. Surface degradation of Al6061/15% SiC/ composite
(a)before eroion-corrosion,
(b) after corrosion, and
(c) after erosion-corrosion

Fig. 15a shows the surface of the Al6061/15%SiC_p composite before erosion corrosion tets. The effect of corrosion on the surface is revealed in Fig. 15b. Pits and grooves can be observed due to the chemical effect of saline water. Fig. 15c shows the effect of erosion corrosion where more grooves, pits, and cutting marks due to shear effect and plastic deformation can be observed. In addition, wider and deeper grooves can be seen in case of Al6061/SiC composites compared to alloy. Due to the existence of SiC particles in Al alloy, small crater and grooves can be seen (Fig. 15c).

3.5.2 Influence of flow velocity on erosion-corrosion at various temperatures

The influences of flow velocity (at various temperatures) on the weight loss due to chemical corrosion and erosion corrosion for both Al6061 alloy and Al6061/15%SiC_p composite are shown in Figs. 16, 17, and 18. Generally, upon increasing the temperature from 30 to 50 and 80 ^oC the erosion corrosion increases. However, the erosion corrosion for Al 6061 alloy is greater than the erosion corrosion for Al6061/15%SiC_p composite under the same conditions. Fig.16 shows the effect of flow velocity on the weight loss at 30 ^oC. It is observed that the erosion corrosion resistance decreases with increasing the flow

velocity for both materials. For Al6061/15%SiCp composite the weight loss due to chemical corrosion increased gradualy from $9.8x10^{-6}$ g/mm^2 to $11.6x10^{-6}$ g/mm^2 (18.5%) with increasing the flow velocity from 1 m/s to 6 m/s. The weight loss due to the combined effect of erosion and corrosion increased from 12 $x10^{-6}$ g/mm^2 to 13.7 $x10^{-6}$ g/mm^2 (14.2%) for the same velocity range. The influences of flow velocity on the erosion corrosion behavior of Al6061 alloy and Al6061/15%SiCp composite at 50 ºC is revealed in Fig.17. It is noticed that the trend of weight loss with respect to the flow velocity is similar to Fig.16. However, with increasing slurry temperature, the weight loss increases for both Al6061 alloy and Al6061/15%SiCp composite. It can be noticed that the weight loss due to chemical corrosion of Al6061/15%SiCp composite increases from $11.2x10^{-6}$ g/mm^2 to $14.3x10^{-6}$ g/mm^2 (27.6%) with increasing the flow velocity from 1 m/s to 6 m/s. The weight loss due to the effect of erosion and corrosion increased from $12.2x10^{-6}$ g/mm^2 to $16.1x10^{-6}$ g/mm^2 (32%) for the same velocity range.

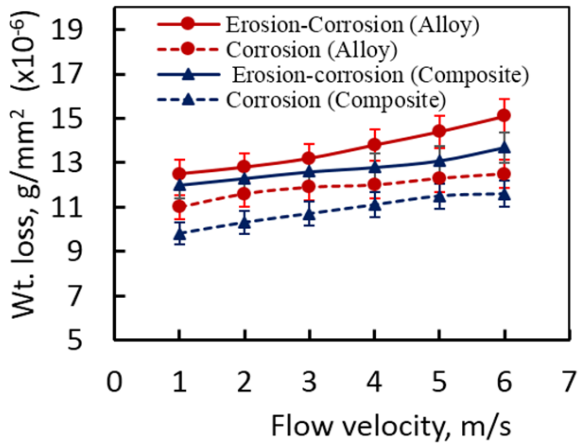

Fig. 16. Velocity effect on weight loss of Al 6061 alloy and Al6061/15%SiC/ composite. (T = 30 ºC)

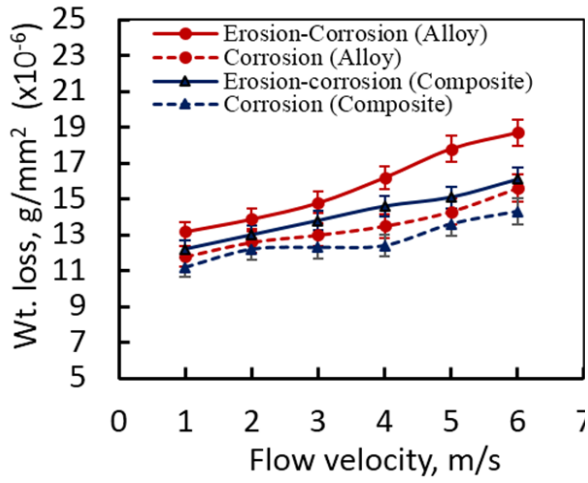

Fig. 17. Velocity effect on weight loss of Al 6061 alloy and Al6061/15%SiC/ composite. (T = 50 ºC)

The influences of flow velocity on the erosion corrosion behavior of Al6061 alloy and Al6061/15%SiCp composite at 80 ºC is shown in Fig.18. It can be seen that the weight loss due to chemical corrosion of Al6061/15%SiCp composite increases from $13.2x10^{-6}$ g/mm^2 to $17.1x10^{-6}$ g/mm^2 (29.5%) with increasing the flow velocity from 1 m/s to 6 m/s. The weight loss due to the effect of erosion and corrosion increased from $14.9x10^{-6}$ g/mm^2 to $20.1x10^{-6}$ g/mm^2 (35%) for the same velocity range. The enhancement in the erosion corrosion resistance of the Al6061/15%SiCp composite rather than the Al6061 alloy is attributed to the high hardness of SiC particles which acts as a reinforcement and obstacle for the erosion corrosion.

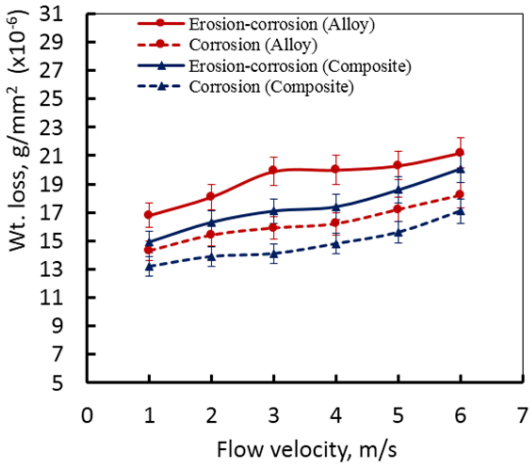

Fig. 18. Velocity effect on weight loss of Al 6061 alloy and Al6061/15%SiC/ composite. (T = 80 ºC)

The micrographs in Fig. 14 and Fig.15 show the effect of SiC reinforcement on the erosion corrosion behavior of Al 6061 alloy . As discussed before the weight losses at different velocities and durations yielded to an improvement in erosion corrosion resistance of Al6061/15%SiC/ composite rather than Al6061 alloy . The micrographs (Figs 14 and 15) approve and show similar trends as presented in Fig. 16 through Fig. 18.

3.5.3 Influence of time on erosion-corrosion at various temperatures

The effect of time (at various temperatures) on the weight loss due to corrosion and erosion corrosion for both Al6061 alloy and Al6061/15%SiCp composite are presented in Figs. 19, 20, and 21. The tests were conducted at duration range from 10 h to 60 h. The constant conditions were a velocity of 6 m/s and sand slurry in water 20 wt.%. The weight loss per unit area with respect to testing durations at 30 ºC is shown in Fig. 19. The results demonstrate that the time of experiment has a considerable effect on erosion corrosion of Al 6061 alloy and Al6061/15%SiC/ composite. Fig.20 and Fig.21 show the weight loss at 50 ºC and 80 ºC. A noticeable weight loss due to erosion corrosion was observed for the 60 h tests. It can be concluded that the increase in hardness due to the presence of SiC particles increases the erosion corrosion resistance of both Al 6061/SiC composite. Furtheremore, the high work hardening was

found to be useful for increasing the erosion corrosion resistance.

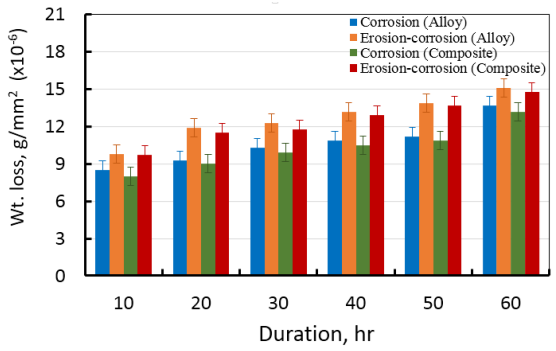

Fig. 19. Time effect on weight loss of Al 6061 alloy and Al6061/15%SiC/ composite. (T = 30 ºC)

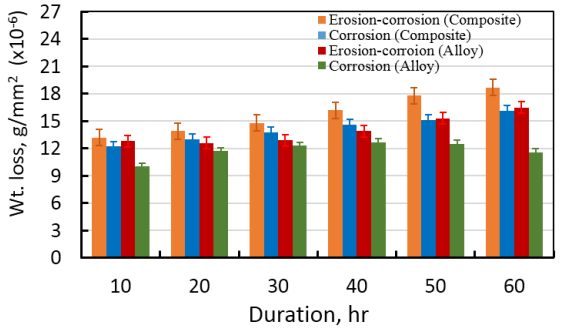

Fig. 20. Time effect on weight loss of Al 6061 alloy and Al6061/15%SiC/ composite. (T = 50 ºC)

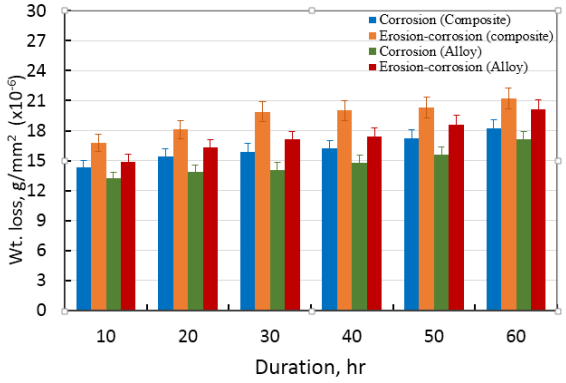

Fig. 21. Velocity effect on weight loss of Al 6061 alloy and Al6061/15%SiC/ composite.(T = 80 ºC)

4. CONCLUSION

The hot deformation of the Al6061/15%SiCp composite was carried out through compression test at the temperature range (300 ºC - 500 ºC) and strain rates (0.008, 0.05, 0.4, and 2.7 s^{-1}). An attempt was made to develop a relationship of the true stress-true strain for the Al/15%SiCp composite at different temperatures. The erosion corrosion tests were also conducted on Al 6061/15% SiCp composite. The highlights of the study can be stated as follows:

1. For Al 6061/15% SiCp composite, the relation between flow stresses with strain rate and temperature are in direct correlation.
2. Increasing the temperature and decreasing strain rate result in reducing the flow stress of the Al 6061/15 vol.% SiCp composite.
3. The regression analysis was used successfully for modeling and comparing the measured and predicted results.
4. The regression method was demonstrated through mathematical equations. By observing the percentage deviation, the utility of the regression model was efficient.
5. The microstructure of the compressed Al 6061/15%SiCp revealed that higher strain rates and temperatures lead to interface cracking.
6. The flow velocity and time of experiemets have substantial effects on the erosion corrosion of Al6061 alloy and Al6061/15%SiCp composite. However, the erosion corrosion resistance of Al6061/15%SiCp composite is more than that for Al6061 alloy. This means that the presence of SiC particles enhances the surface properties of Al6061/SiC composite.

ACKNOWLEDGEMENT

The authors would like to thank both Qassim university , Saudi Arabia and Beni Suef university, Egypt for supporting and facilitating the current work.

REFERENCES

[1] Osama M. Irfan and Hanafy M. Omar, "Experimental Study and Prediction of Erosion-Corrosion of AA6066 Aluminum Using Artificial Neural Network, ***International Journal of Mechanical & Mechatronics Engineering***", 17(6): 1-14, (2017)

[2] Xiao Pu LI., LIU Chong Y., Xiao Wei SUN., Ming Zhen MA., and Ri Ping LIU., "Hot deformation behavior and processing maps of AA6061-10 vol.% SiC composite prepared by spark plasma sintering", ***SCIENCE CHINA Technological Sciences*** 59(6): 980-988, (2016).

[3] Gopalakrishnan S. and Murugan N., "Production and wear characterization of AA 6061-matrix titanium carbide particulate reinforced composite by enhanced stir casting method", ***Compos Part B-Engineering***, 43: 302-308, (2012).

[4] Ashwath P. and Xavior M.A., "Processing methods and property evaluation of Al2O3 and SiC reinforced metal matrix composites based on aluminium 2xxx alloys", ***J. Mater. Res.***, 31: 1201–1219, (2016).

[5] Zhang, Q., Ma X. Y., and Wu G. H., "Interfacial microstructure of SiCp/Al composite produced by the pressureless infiltration technique", ***Ceram Int***, 39: 4893–4897, (2013).

[6] Zhang J. T., Liu L. S., and Zhai P. C., "Effect of fabrication process on the microstructure and dynamic compressive properties of SiCp/Al composites fabricated

by spark plasma sintering", ***Material Letters***, 62: 443–446, (2008).

[7] Reddy P.S., Kesavan R., and Vijaya Ramnath B., "Investigation of mechanical properties of aluminum 6061-silicon carbide, boron carbide metal matrix composite", ***Silicon***, 9: 1–8, (2017).

[8] Tengke Ye, Yuxin Xu, and Jie Ren., "Effects of SiC particle size on mechanical properties of SiC particle reinforced aluminum metal matrix composite", ***Materials Science & Engineering, A*** 753: 146–155, (2019).

[9] Kanhu Charan Nayak and Prashant P. Date., "Hot deformation flow behavior of powder metallurgy based Al-SiC and AlAl2O3 composite in a single step and two-step uni-axial compression", ***Materials Characterization***, 151: 563–581, (2019).

[10] El-Sabbagh A., Soliman M., and Taha M., "Hot rolling behavior of stir-cast Al 6061 and Al 6082 alloys-SiC fine particulates reinforced composites". ***J. Mater Process Tech*** 212: 497–508, (2012).

[11] Taha M. A., El-Mahallawy N. A., and El-Sabbagh A. M., "Some Experimental Data on Workability of Aluminum-Particulate-Reinforced Metal Matrix Composites", ***J. Mater. Process. Techno*** 202 (1–3): 380–385, (2008).

[12] Zabihi, M., Toroghinejad M. R., and Shafyei A., "Application of powder metallurgy and hot rolling processes for manufacturing aluminum/ alumina composite strips", ***Mat Sci Eng A-Struct***. 560: 567–574, (2013).

[13] Agus Pramono, Lembit Kommel, Lauri Kollo, and Renno Veinthal., "The Aluminum Based Composite Produced by Self-Propagating High Temperature Synthesis", ***Materials Science***, 22(1): 41-43, (2016).

[14] Pitchayyapillai G., Seenikannan P., and Raja K., "Chandrasekaran, K. Al6061 hybrid metal matrix composite reinforced with alumina and molybdenum disulphide". ***Adv. Mater. Sci. Eng.***, 2016: 6127624, (2016).

[15] Ch Hima Gireesh, K. G. Durga Prasad, and Koona Ramji, "Experimental Investigation on Mechanical Properties of an Al6061 Hybrid Metal Matrix Composite", ***J. Compos. Sci.***, 2(49): doi:10.3390/jcs2030049, (2018).

[16] Chang, C. I., Lee C. J., and Huang J. C., "Relationship between grain size and Zener–Holloman parameter during friction stir processing in AZ31 Mg alloys", ***Scripta Materialia*** 51: 509–514, (2004).

[17] Sellars C. M., "On physical metallurgy of thermo-mechanical processing of steels and other metals", ***Proc. of Int. Conference THERMEC***, Tokyo, 88:, 448-457, (2011).

[18] Srivatsan T. S. and Prakash A., "The quasi-static fracture behavior of an aluminum alloy metal-matrix composite", ***Composites Science and Technology***, 53: 307–315, (1995).

[19] Dipti Kanta Das, Purna Chandra Mishra, Saranjit Singh, and Swati Pattanaik., "Fabrication and heat treatment of ceramic reinforced aluminum matrix composites – A Review", ***International Journal of Mechanical and Materials Engineering*** 1:6, (2014).

[20] Hung N. P., Boey F. Y. C., Khor K. A., Oh C. A., and Lee H. F., "Machinability of cast and powder-formed aluminum alloys reinforced with SiC particles". ***Journal of Materials Processing Technology***, 48: 291–297, (1995).

[21] Song W. Q., Krauklis P., Mouritz A. P., and Bandyopadhyay S., "The effect of thermal ageing on the abrasive wear behavior of age hardening 2014 Al/ Sic and 6061 Al/SIC composites", ***Wear***, 185: 125–130, (1995).

[22] Kalkanli A. and Yilmaz S., "Synthesis and characterization of aluminum alloy 7075 reinforced with silicon carbide particulates", ***Materials and Design***, 29: 775–780, (2008).

[23] Rao R. N., Das S., Mondal D.P., and Dixit G., "Dry sliding wear behavior of cast high strength aluminum alloy (Al–Zn–Mg) and hard particle composites", ***Wear***, 267: 1688–1695, (2009).

[24] Nagaral M., Auradi V., Parashivamurthy K.I., and Kori S.A., "A Comparative Study on Wear Behavior of Al 6061-6% SiC and Al6061-6% Graphite Composites". J ***Appl Mech Eng*** 5: 227. doi: 10.4172/2168-9873.1000227, (2016).

[25] Nagaral M., Attar S., Reddappa H.N., Auradi V., Kumar S., and Raghu S., "Mechanical behaviour of Al7025-B4C particulate reinforced composites". ***J. Applied Mechanical Engineering***, 4: 6, DOI: 10.4172/2168-9873.1000186, (2015).

[26] Suresh S., Shenbaga V.M., Vettivel S.C., and Selvakumar N., "Mechanical behaviour and wear prediction of stir cast Al-TiB2 composites using response surface methodology", ***Materials and Design***, 59: 383-396, (2014).

[27] Umanath K., Palanikumar K., and Selvamani S.T., "Analysis of dry sliding wear behavior of Al6061-SiC-Al2O3 hybrid metal matrix composites", ***Composites Part-B***, 53:159-168, (2013).

[28] Naveed M. and Khan A.R.A., "Ultimate Tensile Strength of Heat Treated Hybrid Metal Matrix Composites", ***Int. J. Sci. Res***., 4:146–151, (2015).

[29] Chawla K. Fibrous, Materials, 2nd ed., Cambridge University Press: Cambridge, UK, (2016).

[30] Osama M. Irfan, Fahad A. Al-Mufadi, and F. Djavanroodi, "Surface Properties and Erosion–Corrosion Behavior of Nanostructured Pure Titanium in Simulated Body Fluid", ***Metallurgical and Materials Transactions A***, 49A:5695 – 5704, (2018).

[31] Wei S. H., Liu Y. Q., Nie J. H., Zuo T. Z., Ma L., and Fan J. Z., "Hot Deformation Behavior and Processing Map of 25%SiCp/2009A1 Composite", ***Materials Science Forum***, 849: 409-415, (2016).

[32] Sivakesavam O., "Effect of Processing History and Initial Microstructure on the Hot Working of Mg, Mg–Zn–Mn, Mg–Li–Al, and Mg–Li–Al–Zr Alloys: Characterization with Processing Maps" Ph.D. Thesis, ***Indian Institute of Science***, Bangalore, (1994).

[33] Jingli Duan, Yuanbiao Tan, Liyuan Ji, Wenchang Liun, Jing wu Zhang, and Riping Liu., "Hot deformation behavior of 51.1 Zr–40.2 Ti–4.5 Al–4.2 V alloy in the single β phase field", ***Progress in Natural Science, Materials International***, 25:34–41, (2015).

[34] Ganesan G., Raghukandan K., and Karthikeyan R., "Formability study on Al/SiC composites. ***Mater Sci Forum***", 437(438): 227–230, (2003).

[35] Zhang, P., Li F. G., and Wan Q., "Constitutive equation and processing map for hot deformation of SiC particles reinforced metal matrix composites", ***J. Mater Eng Performance***, 19: 1290–1297, (2010).

[36] Zhang H., Lin G. Y., and Peng D. S., "Dynamic and static softening behaviors of aluminum alloys during multistage hot deformation". ***J. Mater Process Tech***, 148: 245–249, (2004).

[37] Li H. Z., Wang H. J., and Zeng M., "Forming behavior and workability of 6061/B4Cp composite during hot deformation", ***Compos Sci Technology***, 71: 925–930, (2011).

[38] Yar A. A., Montazerian M., and Abdizadeh H., "Microstructure and mechanical properties of aluminum alloy matrix composite reinforced with nano-particle MgO", ***J. Alloys Compd***, 484: 400 - 404, (2009).